Modeling the Synergy of Cofilin and Arp2/3 in Lamellipodial Protrusive Activity

Nessy Tania[a,b], John Condeelis[c], and Leah Edelstein-Keshet[a1]

[a]Department of Mathematics,
University of British Columbia, Vancouver, BC V6T 1Z2, Canada

[b] Department of Mathematics and Statistics,
Smith College, Northampton, MA 01063

[c]Department of Anatomy and Structural Biology,
Gruss Lipper Biophotonics Center,
Albert Einstein College of Medicine of Yeshiva University, Bronx, NY 10461

[1]Corresponding author
Email: keshet@math.ubc.ca

Contents

1 Well-Mixed Model

Below we list the full model equations for the well mixed model as discussed in the main paper and simulation results showing response to a transient stimulation.

1.1 Equations

Within a transect of the lamellipod, we keep track of the length density of F-actin filaments (new ATP-F-actin, F_{new}, and old ADP-F-actin, F_{old}) and the corresponding barbed end density B, as well as the concentrations of active cofilin, C, and Arp2/3, A. The definitions and values of parameters are given in Table S1.

New F-actin

$$\frac{dF_{new}}{dt} = J_f - k_{age}\, F_{new} + V_0\, B\,, \tag{S1}$$

Old F-actin

$$\frac{dF_{old}}{dt} = k_{age}\, F_{new} - k_{deg}\, F_{old}\,, \tag{S2}$$

Barbed Ends

$$\frac{dB}{dt} = \kappa(f_{sev}(C, F_{old}) + f_{nuc}(A, F_{new})) - k_{cap} B\,, \tag{S3}$$

Free active cofilin

$$\frac{dC}{dt} = J_C(t) - k_c C - f_{sev}(C, F_{old})\,, \tag{S4}$$

Cofilin severing rate

$$f_{sev}(C, F_{old}) = k_{sev} C_0 \left(\frac{C}{C_0}\right)^n \ell F_{old}\,, \tag{S5}$$

Free active Arp2/3

$$\frac{dA}{dt} = J_A(t) - k_a A - f_{nuc}(A, F_{new})\,, \tag{S6}$$

Arp2/3 binding rate

$$f_{nuc}(A, F_{new}) = k_{nuc} \frac{A}{K_m + A}\, \ell F_{new}\,. \tag{S7}$$

1.2 Additional Simulation Result

Simulation results shown in Fig. S1 are obtained by imposing a 10 s pulse of cofilin activation (step function $J_C(t)$), starting at $t = 2$ s. Cofilin level increases quickly and cofilin binds to old F-actin (F_{old}, initially at its low basal level). After a 5 s delay, the barbed end density increases and peaks at ∼13 s. This leads to the polymerization of new F-actin which achieves its maximum value at approximately 20 s. The new filaments then slowly age to F_{old}. Following stimulation, the system returns to its basal steady state (no active cofilin, no uncapped barbed ends, and low level of F-actin).

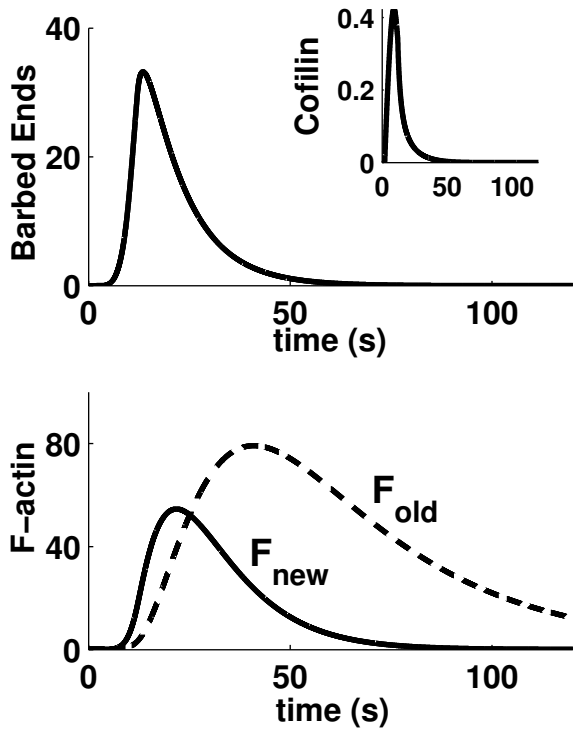

Figure S1: Dynamics of barbed ends, cofilin (inset) and F-actin following a high cofilin stimulus, obtained by a stimulus-induced flux of cofilin into the cell ($J_C = 0.1$ μM/s for $2 \leq t \leq 12$ s). Arp2/3 is absent here. Results are obtained using the basic parameter values listed in Table S1 and steady state initial conditions ($A(0) = 0$, $C(0) = 0$, $B(0) = 0$, $F_{new}(0) = J_f/k_{age}$, $F_{old} = J_f/k_{deg}$).

2 Full Spatial Model

Here we describe the full spatial model. For completeness, we provide the full equations, and details of boundary and initial conditions used. We also derive the coordinate transformation to a moving frame used in all simulations.

2.1 Equations

Length density of new F-actin (unit: $\mu\text{m}/\mu m^2$)

$$\frac{\partial F_{new}}{\partial t} = J_f - k_{age}\, F_{new} + V_0\, B\,, \qquad \text{[S8]}$$

Length density of old F-actin

$$\frac{\partial F_{old}}{\partial t} = k_{age}\, F_{new} - k_{deg}\, F_{old}\,, \qquad \text{[S9]}$$

Density of barbed ends (unit: $\#/\mu\text{m}^2$)

$$\frac{\partial B}{\partial t} = -\frac{\partial}{\partial x}\,(V_0 B) - k_{cap} B + \kappa(f_{sev} + f_{nuc})\,, \qquad \text{[S10]}$$

Concentration of free active Arp2/3 (unit: μM)

$$\frac{\partial A}{\partial t} = -\frac{\partial}{\partial x}\left(V_{mb}\, A\right) - f_{nuc}\left(C, F_{new}\right) - k_a A\,, \qquad \text{[S11]}$$

Concentration of free active cofilin (unit: μM)

$$\frac{\partial C}{\partial t} = D_c \frac{\partial^2 C}{\partial x^2} - \frac{\partial}{\partial x}\left(V_{mb}\, C\right) - f_{sev}\left(C, F_{old}\right) - k_c C\,. \qquad \text{[S12]}$$

Cofilin severing function f_{sev} and Arp2/3 binding rate f_{nuc} as in Eqns. [S5]-[S7].

Pushing barbed ends (unit: $\#/\mu$m)

$$\frac{dB_p}{dt} = (V_0 - V_{mb}) B(x_{edge}, t) - k_{cap} B_p\,, \qquad \text{[S13]}$$

Membrane protrusion rate (unit: μm/s)

$$V_{mb}(B_p) = V_0 \frac{B_p}{B_p + \phi \exp(\omega / B_p)}\,. \qquad \text{[S14]}$$

3 Implementation details for the spatial model

Our spatial model extends and improves that of Dawes et al. (1) for Arp2/3. First, we correct the boundary conditions for barbed ends and actin filaments at the cell edge, as discussed below. In the current formulation, conservation of barbed ends is maintained, and the number of actin filaments at the edge is consistent with the number of pushing barbed ends. Second, we correct the assumption that Arp2/3 can diffuse throughout the lamellipod. To reflect Arp2/3 activation occurring at the cell membrane, we use a Dirichlet boundary condition. We implemented the Arp2/3 PDE with a small "numerical" diffusion coefficient for Arp2/3 to avoid instabilities. This feature restricts Arp2/3 to within 0.1 μm of the cell edge. To reflect the release of active cofilin from its PIP_2 membrane-bound form (2), we used a finite flux boundary condition for cofilin. Details are described below.

3.1 Boundary and Initial Conditions

We impose the following boundary conditions:

- *Far field conditions*:
  For the barbed ends, we assume that inside the cell, far from the cell edge, the density of uncapped barbed ends is zero $B(-\infty, t) = 0$. We assume that there is no active Arp2/3 or cofilin far from the cell edge, $A(-\infty, t) = 0$ and $C(-\infty, t) = 0$. For all numerical simulations presented here, we take a domain of length 4 μm and impose these far field conditions at $x = x_{edge} - 4$ μm.

- *F-actin length density at x_{edge}*:
  The F-actin length density can be interpreted either as length of filaments per unit area (μm/μm^2) or as the number of filaments per μm across the width of the narrow transect ($\#/\mu$m). Right at the cell edge, the number of filaments per unit edge length must match the number of barbed ends per unit edge length, $B_p(t)$. We assume that

these pushing barbed ends are tips on new filaments, so $F_{new}\left(x_{edge}(t),t\right) = B_p(t)$ and $F_{old}\left(x_{edge}(t),t\right) = 0$. Note that these boundary conditions are needed following a coordinate transformation to a moving frame for the purpose of numerical simulation.

- *Activation for cofilin and Arp2/3 at the cell edge*:
  To simulate EGF stimulation, we use Neumann boundary conditions to reflect the release of active cofilin into the cell interior,

$$\left[-D_c\frac{\partial C}{\partial x} + V_{mb}\,C\right]_{x=x_{edge}} = \begin{cases} -J_C < 0 & \text{during stimulation } t \in [t_c, t_c + dt_c] \\ 0 & \text{otherwise,} \end{cases} \qquad \text{[S15]}$$

  Active Arp2/3 is bound to the WAVE2 complex on the cell membrane. We assume that activation simply increases the level of active Arp2/3 at the cell membrane:

$$A(x_{edge},t) = A_{edge}(t), = \begin{cases} A_{edge} > 0 & \text{during stimulation } t \in [t_a, t_a + dt_a] \\ 0 & \text{otherwise.} \end{cases} \qquad \text{[S16]}$$

Initial conditions are taken to be the unstimulated steady state values for cofilin, Arp2/3 and barbed ends:

$$C^{ss}(x) = 0,\ A^{ss}(x) = 0,\ B^{ss}(x) = 0,\ \text{and } V_{mb}^{ss} = 0,\ B_p^{ss} = 0, \qquad \text{[S17]}$$

The F-actin steady state distributions is $F_{new}^{ss} = J_f/k_{age}$ and $F_{old}^{ss} = J_f/k_{deg}$.

3.2 Derivation of Equation for B_p

We now derive the equation for the pushing barbed ends, B_p, based on a conservation principle. In the absence of creation or capping of barbed ends, the *total* number of barbed ends should be conserved. The total number of barbed ends across the lamelipod, including pushing barbed ends is given by

$$B_{total} = \int_{-\infty}^{x_{edge}(t)} B(x,t)dx + B_p(t).$$

To obtain conservation, we must enforce

$$\frac{d}{dt}B_{total} = 0, \quad \Rightarrow \quad \frac{d}{dt}\int_{-\infty}^{x_{edge}(t)} B(x,t)dx = -\frac{d}{dt}B_p(t).$$

Using [S10] and integrating over space, note that

$$\begin{aligned} \frac{d}{dt}\left[\int_{-\infty}^{x_{edge}(t)} B(x,t)dx\right] &= \int_{-\infty}^{x_{edge}(t)} \frac{\partial B}{\partial t}dx \;+\; B(x_{edge}(t),t)\,\frac{dx_{edge}}{dt} \\ &= \int_{-\infty}^{x_{edge}(t)} -V_0\frac{\partial B}{\partial x}dx + V_{mb}\cdot B(x_{edge}(t),t) \\ &= -V_0\Big[B(x_{edge}(t),t) - B(-\infty,t)\Big] + V_{mb}\cdot B(x_{edge}(t),t) \\ &= (V_{mb} - V_0)\,B(x_{edge}(t),t). \end{aligned}$$

Thus for conservation, we arrive at an ODE for the pushing barbed ends, $B_p(t)$,

$$\frac{dB_p}{dt} = (V_0 - V_{mb})B(x_{edge}(t), t). \quad \text{[S18]}$$

Allowing for capping, we obtain Eqn. [S13], and this is used to close the system.

3.3 Arp2/3: Numerical Diffusion

In order to impose the boundary conditions associated with stimulation at the cell edge, we modified the hyperbolic Arp2/3 equation [S11] with numerical diffusion (a common practice in treating such PDEs numerically),

$$\frac{\partial A}{\partial t} = \epsilon \frac{\partial^2 A}{\partial x^2} - \frac{\partial}{\partial x}\left(V_{mb}\, A\right) - f_{nuc}\left(C, F_{new}\right) - k_a A.$$

We chose the value of the small parameter $\epsilon = 0.0001\ \mu\text{m}^2/\text{s}$ such that Arp2/3 is restricted to within a thin region $< 0.1\ \mu$m of the cell edge. This thickness is likely an overestimate. However, it makes computations on a reasonable grid feasible. Later on we discuss how decreasing the region of Arp2/3 influence affects our conclusions.

3.4 Transforming to Moving Coordinate System

For numerical simulations, we change the coordinate system from a static "lab" frame (x, t) to a frame moving with the cell edge, $(z(t), t)$ where $z(t) = x - x_{edge}(t)$ is a position relative to the cell edge. Then, for any function $G(z(t), t)$, the rate of change is given by the material derivative,

$$\frac{DG}{Dt} = \frac{\partial G}{\partial t} + \frac{\partial G}{\partial z}\cdot\frac{dz}{dt} = \frac{\partial G}{\partial t} - \frac{\partial G}{\partial z}\cdot\frac{dx_{edge}}{dt} = \frac{\partial G}{\partial t} - V_{mb}(t)\frac{\partial G}{\partial z}. \quad \text{[S19]}$$

Note that here, V_{mb} is not constant nor prescribed a priori, and that it depends on the number of pushing barbed ends (Eqs. [S13]-[S14]), itself a dynamic variable. Following this formal change of coordinate, the cell edge corresponds to $z = 0$. The full system now can be written as,

$$\begin{aligned}
\frac{\partial B}{\partial t} &= -\frac{\partial}{\partial z}\Big[(V_0 - V_{mb})B\Big] - k_{cap}\, B + \kappa(f_{sev} + f_{nuc}), && \text{[S20]}\\
\frac{\partial F_{new}}{\partial t} &= V_{mb}\,\frac{\partial F_{new}}{\partial z} + V_0\, B - k_{age}\, F_{new}, && \text{[S21]}\\
\frac{\partial F_{old}}{\partial t} &= V_{mb}\,\frac{\partial F_{old}}{\partial z} + k_{age}\, F_{new} - k_{deg}\, F_{old}, && \text{[S22]}\\
\frac{\partial C}{\partial t} &= D_c\frac{\partial^2 C}{\partial z^2} - f_{sev}\left(C, F_{old}\right), && \text{[S23]}\\
\frac{\partial A}{\partial t} &= \epsilon\frac{\partial^2 A}{\partial z^2} - f_{nuc}\left(C, F_{old}\right), && \text{[S24]}
\end{aligned}$$

where variables are now functions of both $z(t)$ and t. It is interesting to note that this set of equations describes an "apparent" drift of F-actin rearwards (as it is left behind when the

cell edge moves forward), a motion of barbed ends towards the cell edge (with relative speed $(V_0 - V_{mb})$) and simple diffusion of cofilin. The numerical Arp2/3 diffusion is also preserved.

Numerical approximation of the solution of this system is obtained by discretizing using a finite difference scheme. Diffusion terms are discretized using a Crank-Nicolson method and advection terms are discretized using an explicit first-order upwind scheme. Reaction terms are implemented explicitly in the discretized system. Our computational domain reflects the first 4 μm from the cell edge. We chose a spatial step size of $\delta x = 4/2000 = 0.002$ μm, and a time-step of $\delta t \leq 0.001$ s is chosen for stability.

4 Parameter Estimation

In Table S1, we list the parameter values and their sources. The values are inferred from existing literature as discussed below.

4.1 Actin Dynamics Parameters

We assume that over the timescale of the stimulation, monomer availability is not limiting, so that polymerization velocity is roughly constant. We take $V_0 \approx 0.3$ μm/s, a typical value as estimated in (3, 4).

We make a simplifying assumption that capping of barbed ends occurs at an equal rate everywhere. In (3), it was estimated that at a typical cellular concentration of capping protein, a free barbed end has a half life of ~ 0.25 s before being capped (maximum capping rate of $\ln(2)/0.25$ s ≈ 2.77/s). However, barbed-end capping near the membrane is reduced to $\sim$0.1/s. Here we assume $k_{cap} = 1$/s as in (1).

Full ATP to ADP actin conversion takes 10-30 s (3), and we take $k_{age} = 0.1$/s. The half life of actin filaments within the lamellipodia of fibroblasts, fish keratocytes and nerve growth cones is estimated to be 0.5-3 min ((3, 11)), we take $k_{deg} = \ln(2)/23$ s ≈ 0.03/s (1, 5). This parameter reflects a combined turnover rate of F-actin and includes various cofilin-independent processes such as depolymerization, debranching, and fragmentation.

The parameters ω and ϕ describing the dependence of the protrusion rate V_{mb} on the number of pushing barbed ends, were taken directly from (6) (see equation (24) in their Supplementary Material for derivation and discussion).

In this model, we assume that there is no cofilin and Arp2/3 activity when the cell is at rest (basal unstimulated state). Thus, we assume a very low density of F-actin at rest, attributed to de-novo nucleation by other sources such as formin (12), taking $J_f = 0.01/\mu$m s.

4.2 Scale Factors

We consider a 1 μm-wide transect of a lamellipod that has constant thickness 0.18 μm, and length 10 μm (13). The units for cytoskeletal variables (F-actin and barbed ends) are number or length per unit area averaged over the thickness of the transect. The constant κ represents a scale factor for change of units between concentration, in μM, and barbed end density, B, in $\#/\mu\text{m}^2$. A concentration of 1 μM corresponds to 602 molecules/μm^3.

Table S1: List of parameter values and their sources. E_0: primary experimental literature, M: pre-existing models, E_2: values used in previous models but based on experimental literature.

Parameters	Definitions	Values	Source
V_0	free polymerization speed	0.3 μm/s	E_0: (3, 4)
k_{cap}	capping rate	1 /s	M, E_2: (1)
k_{age}	rate of filament aging	0.1 /s	E_0: (3)
k_{deg}	bulk filament turnover rate	0.03 /s	E_0, M: (1, 3, 5)
ω	physical parameter describing membrane resistance	50 /μm	E_0: (6)
ϕ	geometric parameter used in computing protrusion rate	10 /μm	E_0, M: (6)
J_f	basal actin nucleation rate	0.01 /μm.s	M: small value
D_c	diffusion coefficient of cofilin	10 μm^2/s	E_0, M: (5, 7)
ϵ	numerical diffusion coefficient of Arp2/3	0.0001 μm^2/s	this paper
κ	scale factor converting concentrations to units of B	106 /μm$^2 \cdot \mu$M	M: (5)
ℓ	scale factor converting units of F to concentration	0.255 μM·μm	M: (5)
k_{nuc}	Arp2/3 nucleation rate	60/ℓ /s	E_2, M: (5)
K_m	saturation constant for Arp2/3 nucleation	2 μM	M: (5)
k_{sev}	severing rate for cofilin	0.01/μM·s	E_0: (8, 9)
C_0	threshold for cofilin cooperative severing	0.1 μM	E_0: (8, 9)
n	degree of cofilin cooperative severing	4	M: (10)
k_a	basal Arp2/3 degradation rate	0.1/s	M: (5)
k_c	basal cofilin degradation rate	0.1/s	M: (10)
J_c	Inward active cofilin edge flux	0-10 μM·μm/s	values varied
A_{edge}	Active Arp2/3 edge concentration	0-10 mM	values varied

Assuming a lamellipodium of thickness 0.18 μm, a concentration of 1 μM gives $\kappa = 0.18\ \mu\text{m} \cdot (602\ \text{molecules}/\mu\text{m}^3)/(1\mu\text{M}) \approx 106\ \text{molecules}\ /\mu\text{m}^2 \cdot \mu\text{M}$.

The scale factor ℓ is used to convert units of F-actin (length per unit area, $\mu\text{m}/\mu\text{m}^2 = \mu\text{m}^{-1}$) to that of Arp2/3 concentration (5). As derived for κ, we take 1 μM of actin to correspond to 106 monomers/μm^2 lamellipodial area. Now, one monomer contributes to 0.027 μm of filament length. Thus, 1 μm of filament length per 1 μm^2 area corresponds to $1/(0.027 \times 106) = 0.349$ μM of monomers. A minimal distance of approximately 37 nm (23.7 monomers) has been observed between side branches along a single filament (14, 15), so 1μM Arp2/3 approximately binds to 13.7 μM of F (expressed in terms of monomers). Thus, the scale factor for the conversion between F-actin length density to Arp2/3 concentration is $\ell = 0.349/13.7 = 0.255$ μM μm.

Although, the scale factor ℓ just derived takes into account the minimal distance between branches nucleated by Arp2/3 along a filament, for simplicity, we use the same conversion factor ℓ to scale between F-actin and cofilin concentration. The minimal distance between cofilin binding sites along an actin filament can vary. A recent model proposed that multiple cofilin molecules bind cooperatively along an F-actin filament (8, 16). The binding of the first cofilin molecule is slow and dependent upon the fluctuations along the filament, but this then allows rapid subsequent cofilin binding. Boundaries are created between "cofilin-decorated" sections which then promotes severing (8, 16). We do not take into account the physical details of cofilin binding and severing.

4.3 Cofilin and Arp2/3 Parameters

The diffusion coefficient of G-actin (molecular weight of 40 kDa) in the cytosol has been estimated to be 5 μm^2/s (5, 17). Here we take the diffusion coefficient of the smaller protein, cofilin (21 kDa (7)) to be 10 μm^2/s.

The cofilin severing function f_{sev} is discussed in (10), but here parameter values are based on previous in vitro studies (9) and a recent stochastic model of actin length regulation in the presence of cofilin (8). In our model, we take C_0, the threshold for cofilin cooperative severing to be 0.1 μM, based on the dissociation constant for amoeba cofilin bindin to ADP-actin in vivo (9). This value also falls between the dissociation constant of the first cofilin binding ($K_d = 0.59$ μM) and the dissociation constant for the cooperative binding ($K_d^{coop} = 0.067$ μM) given in the detailed stochastic binding model (8). We take a characteristic actin monomer concentration where filaments grow (rather than depolymerize) to be 1 μM, and take the severing rate to be $k_{sev} = 0.01$/s (per μM actin) as in (8).

We assume the same Arp2/3 binding kinetics as in (5). The Arp2/3 nucleation function f_{nuc} is based on a quasi steady state approximation of the following reaction scheme

$$A + \ell F_{new} \underset{k_-}{\overset{k_+}{\rightleftharpoons}} C \xrightarrow{k_2} \ell F_{new} + \kappa B\,, \qquad \text{[S25]}$$

with the assumption that Arp2/3 is a limiting factor (then $K_m = k_-/k_+$ and $k_{nuc} = k_2$). We take a small Arp2/3 inactivation rate, $k_a = 0.1$/s as in (5) and a similar value for for cofilin ($k_c = 0.1$/s); this value is within the range obtained from data-fitting in (10).

5 Spatial Distribution of Barbed End Production

Spatial distribution of severing (f_{sev}) and nucleation (f_{nuc}) rates over time are shown in Fig. S2. The spatial extent of cofilin ($\sim 1\ \mu$m) is an order of magnitude larger than that of Arp2/3 in our model, though both peak at the cell edge.

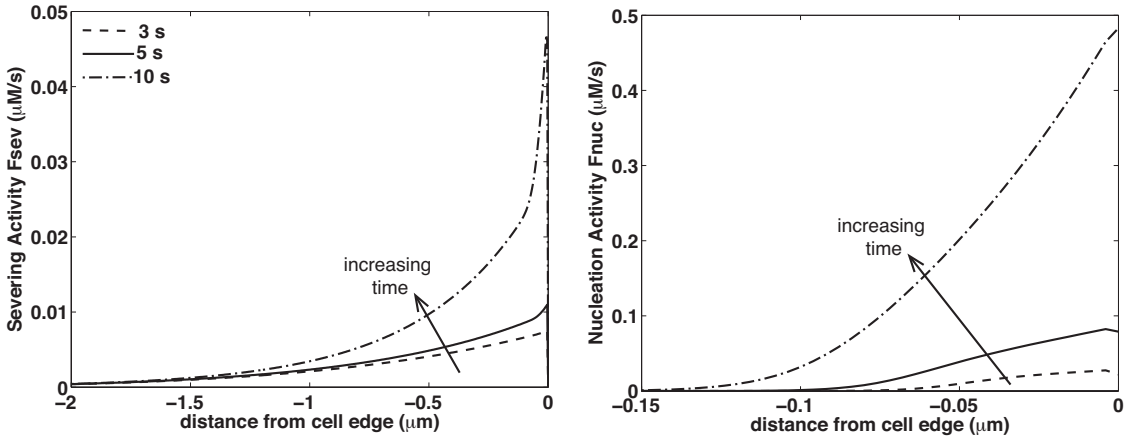

Figure S2: Spatially distributed production of barbed ends: severing by cofilin $f_{sev}(x,t)$ (left), and branching by Arp2/3, $f_{nuc}(x,t)$ (right), at several time points during simulation. Parameters, boundary and initial conditions as in Fig. 3.

6 Effect of Tropomyosin

We considered the effect of tropomyosin which has been shown to compete with cofilin for binding sites along old ADP-F-actin and then protect the filament from severing by cofilin (18). DesMarais et al. (19) showed that level increases from the cell front to the interior (4.5 μm inside) with very little tropomyosin found near the very cell edge.

We incorporated these effects into our mathematical model using the simplest possible assumption to avoid significantly expanding the model. We assume that tropomyosin binding removes available cofilin binding sites on old F-actin, so now

$$\frac{\partial F_{old}}{\partial t} = k_{age}\, F_{new} - (k_{deg} + d_T(x))F_{old}\,, \qquad \text{[S26]}$$

where $d_T(x)$ represents a spatial distribution of tropomyosin which we take to be a linear function (as shown in the top panel of Fig. S3A) similar to the data in (19). We also tracked a third class of F-actin, namely the tropomyosin-protected filaments, F_{tm}.

$$\frac{\partial F_{tm}}{\partial t} = d_T(x)F_{old}\,. \qquad \text{[S27]}$$

In constructing $d_T(x)$, we have chosen a binding rate $T = 5/\text{s}$ away from the cell edge (at 4 μM inside). Wegner and Ruhnau (20) found that at 10 μM tropomyosin concentration, the association rate constant were 2.5-4/μM·s.

The effect of tropomyosin in localizing and limiting the cofilin response are shown in simulation results of Fig. S3. In the bottom panel of Fig. S3A, we plotted the severing rate f_{sev} across the lamellipodial transect at 10 s after stimulation. We found that in the presence of tropomyosin, cofilin activity is reduced, resulting in lower f_{sev} values and that severing activity is more localized towards the front of the cell. While peak severing activity is found at the cell edge with or without tropomyosin, the cofilin activity is contained to within 0.5 μm from the edge in the presence of tropomyosin.

In Fig. S3B, we show the barbed end production curves for cofilin or Arp2/3 acting alone, in the presence/absence of tropomyosin. In this model variant, tropomyosin only affects cofilin activity and its effect on Arp2/3 (21) has not been included. Barbed end production by cofilin is reduced in the presence of tropomyosin. However, the shape of the barbed end production curve with wide sensitive region is retained and thus high synergy and large barbed end production can still be obtained.

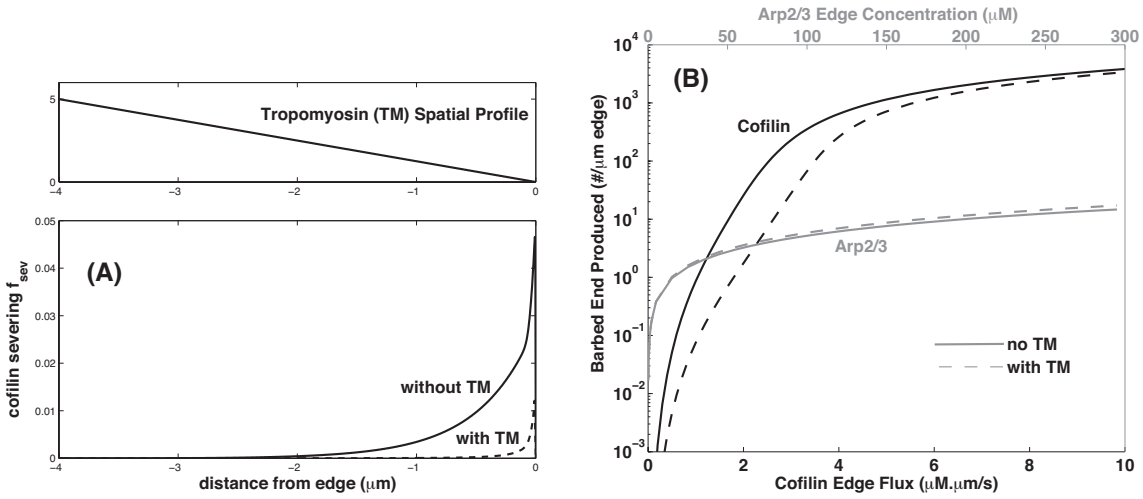

Figure S3: Effects of tropomyosin. **(A)** Top: Assumed spatial profile of tropomyosin in the revised model. Bottom: Rate of barbed end creation by cofilin severing of actin, f_{sev}, across the lamellipod at 10 s after stimulation (with and without tropomyosin). **(B)** The effect of cofilin (Arp2/3) activation release flux at the membrane on barbed end production by cofilin (Arp2/3) acting alone. A qualitatively similar barbed end production is obtained despite tropomyosin inhibition of cofilin. (Compare to Fig. 4A in main paper.)

7 Parameter Sensitivity Tests

Here we report the effects of varying several key parameters, including the F-actin aging rate k_{age}, the barbed end capping rate k_{cap}, and the free polymerization rate V_0.

7.1 Effect of Filament Aging Rate k_{age}

Although the ATP nucleotide is not essential for polymerization of monomers into F-actin (22), its hydrolysis and phosphate dissociation is a "timer" for filament age (4). Once an ATP-G-actin monomer is assembled onto an F-actin polymer, ATP hydrolysis to ADP-Pi is fast (1-3 s (23)). Phosphate (Pi) release, resulting in ADP-F-actin, occurs more slowly (minutes in vitro (24, 25)). Recent studies using microfluidics in the presence of profilin, suggest that Pi release occurs stochastically with a half-life of 102 s (26). However, it has been suggested that Pi release occurs 10 times faster in vivo (3). Cofilin appears to accelerate the release of the phosphate group (9, 27).

We tested the effect of the filament aging timescale. Here we assume that cofilin binds only to ADP-F-actin and Arp2/3 to ATP-F-Actin. In Fig. S4 we show how varying k_{age} in [S8]-[S9] affects barbed end production and synergy. On the left panel, we show barbed end production B_{prod} in the presence of either cofilin or Arp2/3 alone. As k_{age} increases, cofilin severing activity increases because the level of old F-actin increases (making more substrate available for cofilin binding and severing). On the other hand, as k_{age} increases, barbed end production due to Arp2/3 nucleating decreases. On the right panel of Fig. S4, we show barbed end production and synergy in the presence of both cofilin and Arp2/3. Barbed end production increases monotonically with k_{age} and the contribution from cofilin dominates for large k_{age}. However, maximum synergy occurs when $k_{age} \approx 0.12$/s which, interestingly, coincides with the k_{age} rate observed in vivo.

7.2 Effect of Barbed End Capping Rate k_{cap}

Increasing the capping rate, k_{cap}, reduces barbed end production (Fig. S5). We first considered the case when cofilin or Arp2/3 act alone. In that case, we find that barbed end production by Arp2/3 decreases as k_{cap} is increased. Faster capping leads to an overall reduction in the level of new filaments. However barbed end production is not affected significantly when cofilin or Arp2/3 act alone. Doubling the capping rate k_{cap} from 0.1/s to 0.2/s leads only to a 2% (3%) decrease in barbed end production for Arp2/3 (cofilin). However, when cofilin and Arp2/3 work together, capping affects barbed end production significantly. Doubling the capping rate k_{cap} from 0.1/s to 0.2/s leads to a 30% decrease in total barbed end production. This in turn affects cell protrusion as indicated by a sharp decrease in the maximal protrusion rate (a decrease from 0.07 μm/2 to 0.002 μm/s). Synergy also decreases monotonically as k_{cap} is increased (S drops from 4.8 to 3.8 when k_{cap} is doubled from 0.1/s to 0.2/s).

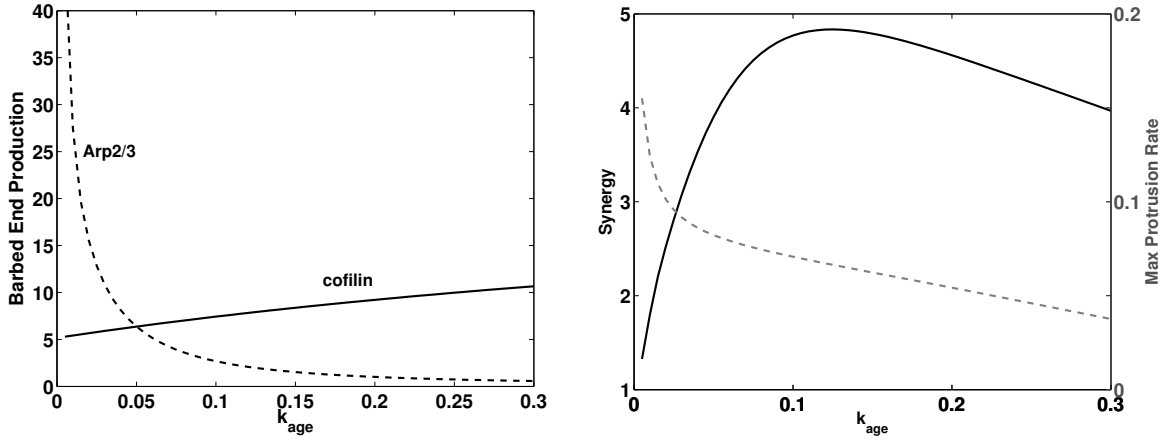

Figure S4: Effect of the F-actin aging rate k_{age} on barbed end production and synergy. Left: Barbed end production (B_{prod}) in the presence of cofilin only (solid curve) and Arp2/3 only (dashed curve). Right: Synergy (black solid curve, left axis) and barbed end production (grey dashed curve, right axis) in the presence of both cofilin and Arp2/3. ($J_C = 1.6$ μM·μm/s, $A_{edge} = 44$ μM, as in Fig. 3), simultaneous cofilin and Arp2/3 stimulation ($0 < t < 10$s). Other parameters as in Table S1.

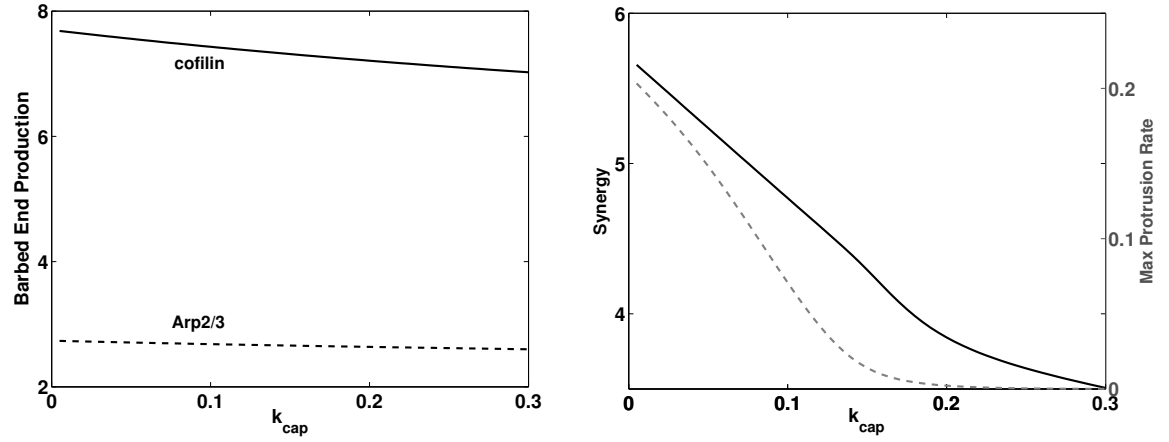

Figure S5: Effect of barbed end capping rate k_{cap} on barbed end production and synergy. Left: Barbed end production (B_{prod}) in the presence of cofilin alone (grey dashed curve, right axis) and Arp2/3 alone (black solid curve, left axis). Right: Synergy (black solid curve, left axis) and barbed end production (grey dashed curve, right axis) in the presence of both cofilin and Arp2/3. ($J_C = 1.6$ μM·μm/s, $A_{edge} = 44$ μM, as in Fig. 3), simultaneous cofilin and Arp2/3 stimulation ($0 < t < 10$s). Other parameters as in Table S1.

7.3 Capping, Aging and Polymerization Speed

We vary capping, filament aging and polymerization speed over a wide range of biologically relevant values, and show the resultant synergy and barbed end production in Fig. S6. Varying k_{cap} and k_{age} (top panels), we find higher barbed end production when k_{cap} is low (slow capping), consistent with previous results of Fig. S5. However, at a given capping rate, high synergy is only found when the filament aging rate, k_{age} is low (slow aging). For the given stimulation size, barbed end production is dominated by Arp2/3. Cofilin simply primes the system by generating new F-actin. We varied the polymerization speed V_0 and capping rate k_{cap} (middle panels). Increasing the polymerization speed increases both synergy and barbed end production. As before, slower capping promotes actin growth. A similar trend is observed when we vary both polymerization speed and filament aging rate (bottom panels).

To summarize, slower caping and filament aging increase both barbed end production and the level of synergy between cofilin and Arp2/3. Faster polymerization speed increases actin growth as well. However, polymerization speed is limited by availability of G-actin monomer, a factor that is not currently represented in our model.

7.4 Arp2/3 Localization parameter (ϵ)

As previously discussed, numerical diffusion (parameter ϵ) in the Arp2/3 equation is used to avoid discontinuities and singularities from developing in the numerical solution. Using a very small value of ϵ then mandates a very fine spatial grid, which increases computation time prohibitively. For this reason, we carried out only limited tests with a reduced value of $\epsilon = 10^{-6}$ μm/s, where Arp2/3 is highly localized to well within 0.01 μm of the cell edge as shown in Movie S3. Barbed end production and synergy results are shown in Fig. S7. From the barbed end production curve, we observe that a much higher Arp2/3 edge-concentration is required to generate a given number barbed ends. Additionally, narrow localization of Arp2/3 limits barbed end production that can be attained; the maximal (plateau) barbed end production level obtained is approximately one order of magnitude lower in comparison to that obtained using ($\epsilon = 10^{-4}$). When Arp2/3 and cofilin are both present, synergy occurs allowing Arp2/3 to generate more barbed ends. From our numerical simulation, the maximal level of synergy observed is ~ 2.6 ($A_{edge} = 2000$ and $J_c = 4$) but this stimulation amplitude leads to low maximum protrusion rate (0.01μm/s). High barbed end production and high synergy can be obtained still by increasing the cofilin edge flux slightly, as shown in the right panel of Fig. S7 ($V_{max} = 0.11$ μm/s here).

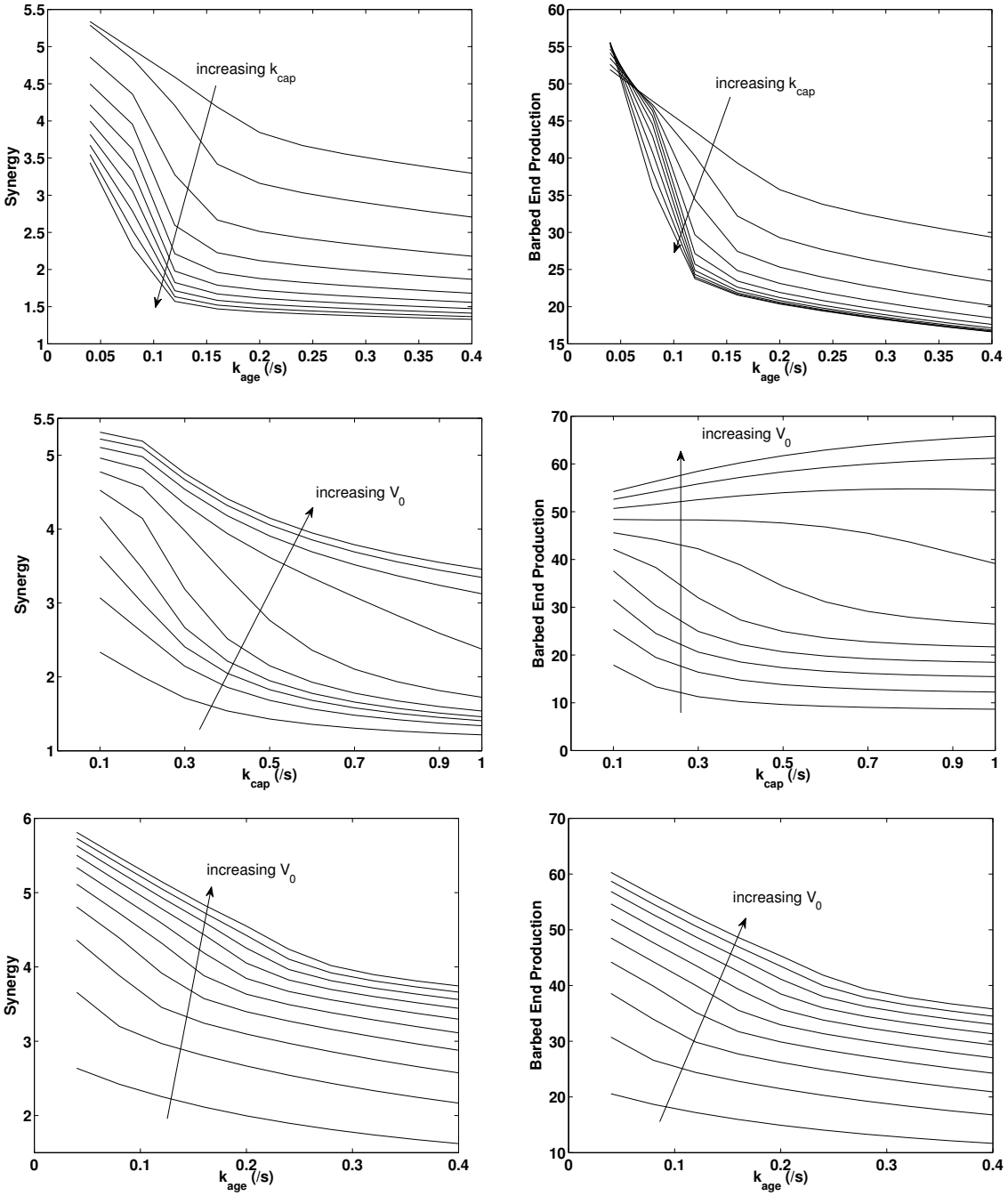

Figure S6: Effects of caping rate k_{cap}, filament aging rate k_{age}, and polymerization speed V_0 on synergy (left panels) and total barbed end production (right panels) ($J_C = 1.6$ μM·μm/s, $A_{edge} = 44$ μM, simultaneous cofilin and Arp2/3 activation for 10 s, but k_{cap}, k_{age} and V_0 varied. Other parameters as in Table S1).

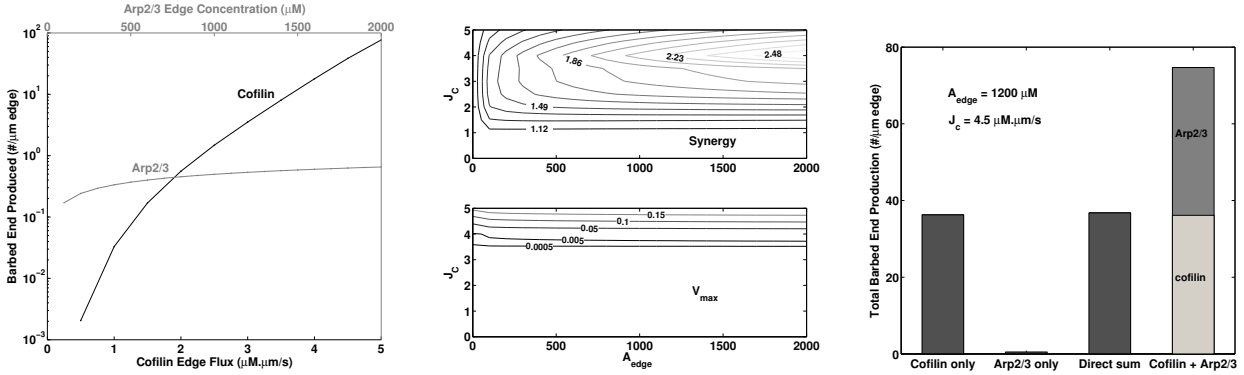

Figure S7: Barbed end production and synergy with highly localized Arp2/3 ($\epsilon = 10^{-6}$ μm/s). Left: Barbed end production curve when cofilin and Arp2/3 act alone. Middle: Synergy and maximum protrusion rate for varying stimulation amplitude. Right: Comparison of total barbed end production using stimulation size of $A_{edge} = 1200$ and $J_c = 4.5$ (S=2.03).

8 Effect of Cofilin Binding to New Filaments

Previous work found that cofilin binds slowly to new F-actin, accelerates release of the phosphate group on ADP-Pi actin filaments (27) and thereby promotes debranching and Arp2/3 dissociation from older filaments (27, 28). Here we explored only the effect of cofilin severing new filaments, rather than its influence on filament aging. This extension can be explored in the future.

Our approach parallels the treatment of Arp2/3 binding, as in Eqn. [19] in the main manuscript. We modified the cofilin severing term to

$$f_{sev}(C, F_{new}, F_{old}) = (1-\beta)k_{sev}C_0\left(\frac{C}{C_0}\right)^n \ell F_{old} + \beta k_{sev}C_0\left(\frac{C}{C_0}\right)^n \ell F_{new}\,. \qquad \text{[S28]}$$

where $0 \leq \beta \leq 1$ reflects preferential binding of cofilin to new versus old F-actin. When $\beta = 0$, cofilin only binds to F_{old} as in our previous basic model. When $\beta > 0$, cofilin can also sever new filaments.

Dependence on β is illustrated in Fig. S8. Neither synergy nor barbed end production is affected significantly as β is varied. As β increases, barbed end production (as reflected by the protrusion rate) slightly increases up to $\beta \approx 0.6$ then slightly decreases thereafter. A higher level of new F-actin is found at the cell edge where cofilin is also activated; thus cofilin can sever more filaments and generate more barbed ends. At high value of β, barbed end production decreases because the older filaments are no longer effective substrate for cofilin severing activity.

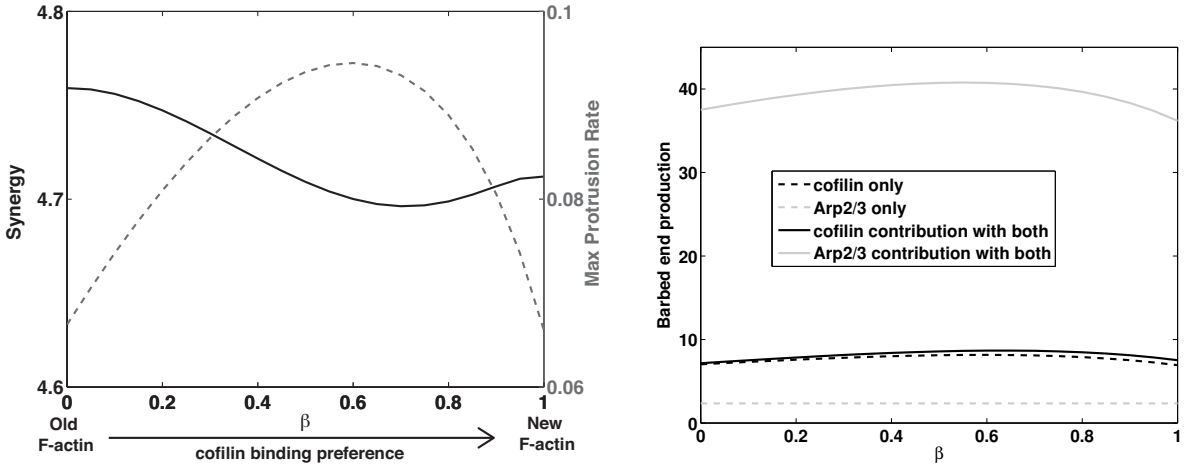

Figure S8: Effect of Cofilin binding to new (ATP) versus old (ADP) F-actin, depicted by β in Eqn. [S28]. Left: Maximum protrusion rate V_{max} (in dashed grey, right axis) and synergy (in solid black, left axis) versus β. Right: Comparison of barbed end production by cofilin ($\int\int f_{sev}\, dxdt$) and by Arp2/3 ($\int\int \overline{f_{nuc}}\, dxdt$) as β is varied. ($J_C = 1.6$ μM·μm/s, $A_{edge} = 44$ μM, simultaneous cofilin and Arp2/3 activation for 10 s, but with Arp2/3 barbed end production rate defined in Eqn. [S28]. Other parameters as in Table S1).

9 List of Movies

- **Movie 1** - Spatio-temporal dynamics of variables following simultaneous cofilin and Arp2/3 stimulation. This movie is analogous to Fig. 3. Top panel: F_{new} is solid line and F_{old} in dashed line.

- **Movie 2** - Spatio-temporal dynamics of variables following a cofilin activation and a delayed Arp2/3 stimulation (t_{arp}=11.5 s). Parameter values as in Fig. 5 B. Top panel: F_{new} is solid line and F_{old} in dashed line.

- **Movie 3** - Spatio-temporal dynamics of variables following simultaneous cofilin and Arp2/3 stimulation obtained using $\epsilon = 10^{-6}$ leading to narrow Arp2/3 localization near the cell edge. This movie corresponds to the right panel of Fig. S7 ($A_{edge} = 1200\mu$m and $J_C = 4.5\mu$M.μm/s. All other parameter values are as listed in Table S1). Top panel: F_{new} is solid line and F_{old} in dashed line.

References

1. Dawes, A. T., G. Bard Ermentrout, E. N. Cytrynbaum, and L. Edelstein-Keshet, 2006. Actin filament branching and protrusion velocity in a simple 1D model of a motile cell. *J Theor Biol.* 242:265–79.

2. van Rheenen, J., X. Song, W. van Roosmalen, M. Cammer, X. Chen, V. Desmarais, S.-C. Yip, J. M. Backer, R. J. Eddy, and J. S. Condeelis, 2007. EGF-induced PIP2 hydrolysis releases and activates cofilin locally in carcinoma cells. *J Cell Biol.* 179:1247–59.

3. Pollard, T. D., L. Blanchoin, and R. D. Mullins, 2000. Molecular mechanisms controlling actin filament dynamics in nonmuscle cells. *Annu Rev Biophys Biomol Struct.* 29:545–76.

4. Pollard, T., and G. Borisy, 2003. Cellular motility driven by assembly and disassembly of actin filaments. *Cell.* 112:453–465.

5. Marée, A., A. Jilkine, A. Dawes, V. Grieneisen, and L. Edelstein-Keshet, 2006. Polarization and movement of keratocytes: a multiscale modelling approach. *Bull Math Biol.* 68:1169–1211.

6. Lacayo, C. I., Z. Pincus, M. M. VanDuijn, C. A. Wilson, D. A. Fletcher, F. B. Gertler, A. Mogilner, and J. A. Theriot, 2007. Emergence of large-scale cell morphology and movement from local actin filament growth dynamics. *PLoS Biol.* 5:e233.

7. Nishida, E., S. Maekawa, and H. Sakai, 1984. Cofilin, a protein in porcine brain that binds to actin filaments and inhibits their interactions with myosin and tropomyosin. *Biochemistry-US.* 23:5307–5313.

8. Roland, J., J. Berro, A. Michelot, L. Blanchoin, and J.-L. Martiel, 2008. Stochastic Severing of Actin Filaments by Actin Depolymerizing Factor/Cofilin Controls the Emergence of a Steady Dynamical Regime. *Biophys J.* 94:2082 – 2094.

9. Blanchoin, L., and T. D. Pollard, 1999. Mechanism of Interaction of Acanthamoeba Actophorin (ADF/Cofilin) with Actin Filaments. *J Biol Chem.* 274:15538–15546.

10. Tania, N., E. Prosk, J. Condeelis, and L. Edelstein-Keshet, 2011. A temporal model of cofilin regulation and the early peak of actin barbed ends in invasive tumor cells. *Biophys J.* 100:1883 – 1892.

11. Welch, M. D., and R. D. Mullins, 2002. Cellular Control of Actin Nucleation. *Annu Rev Cell Dev Bio.* 18:247–288.

12. Zigmond, S. H., 2004. Formin-induced nucleation of actin filaments. *Curr Opin Cell Biol.* 16:99 – 105.

13. Abraham, V. C., V. Krishnamurthi, D. L. Taylor, and F. Lanni, 1999. The Actin-Based Nanomachine at the Leading Edge of Migrating Cells. *Biophys J.* 77:1721 – 1732.

14. Mullins, R. D., J. A. Heuser, and T. D. Pollard, 1998. The interaction of Arp2/3 complex with actin: Nucleation, high affinity pointed end capping, and formation of branching networks of filaments. *Proc Natl Acad Sci USA.* 95:6181–6186.

15. Svitkina, T., and G. Borisy, 1999. Arp2/3 complex and actin depolymerizing factor/cofilin in dendritic organization and treadmilling of actin filament array in lamellipodia. *J Cell Biol.* 145:1009.

16. De La Cruz, E., and D. Sept, 2010. The kinetics of cooperative cofilin binding reveals two states of the cofilin-actin filament. *Biophys J.* 98:1893 – 1901.

17. Novak, I., B. Slepchenko, and A. Mogilner, 2008. Quantitative analysis of g-actin transport in motile cells. *Biophys J.* 95:1627–1638.

18. Ono, S., and K. Ono, 2002. Tropomyosin inhibits ADF/cofilin-dependent actin filament dynamics. *J Cell Biol.* 156:1065–1076.

19. DesMarais, V., I. Ichetovkin, J. Condeelis, and S. E. Hitchcock-DeGregori, 2002. Spatial regulation of actin dynamics: a tropomyosin-free, actin-rich compartment at the leading edge. *J Cell Sci.* 115:4649–4660.

20. Wegner, A., and K. Ruhnau, 1988. Rate of binding of tropomyosin to actin filaments. *Biochemistry-US.* 27:6994–7000.

21. Blanchoin, L., T. D. Pollard, and S. E. Hitchcock-DeGregori, 2001. Inhibition of the Arp2/3 complex-nucleated actin polymerization and branch formation by tropomyosin. *Curr Biol.* 11:1300 – 1304.

22. De La Cruz, E., A. Mandinova, M. Steinmetz, D. Stoffler, U. Aebi, and T. Pollard, 2000. Polymerization and structure of nucleotide-free actin filaments. *J Mol Biol.* 295:517–526.

23. Blanchoin, L., and T. Pollard, 2002. Hydrolysis of ATP by polymerized actin depends on the bound divalent cation but not profilin. *Biochemistry-US.* 41:597–602.

24. Carlier, M., and D. Pantaloni, 1986. Direct evidence for ADP-Pi-F-actin as the major intermediate in ATP-actin polymerization. Rate of dissociation of Pi from actin filaments. *Biochemistry-US.* 25:7789.

25. Melki, R., S. Fievez, and M.-F. Carlier, 1996. Continuous monitoring of pi release following nucleotide hydrolysis in actin or tubulin assembly using 2-amino-6-mercapto-7-methylpurine ribonucleoside and purine-nucleoside phosphorylase as an enzyme-linked assay. *Biochemistry-US.* 35:12038–12045.

26. Jégou, A., T. Niedermayer, J. Orbán, D. Didry, R. Lipowsky, M. Carlier, and G. Romet-Lemonne, 2011. Individual actin filaments in a microfluidic flow reveal the mechanism of ATP hydrolysis and give insight into the properties of profilin. *PLOS Biol.* 9:e1001161.

27. Blanchoin, L., T. Pollard, and R. Mullins, 2000. Interactions of ADF/cofilin, Arp2/3 complex, capping protein and profilin in remodeling of branched actin filament networks. *Curr Biol.* 10:1273–1282.

28. Chan, C., C. C. Beltzner, and T. D. Pollard, 2009. Cofilin Dissociates Arp2/3 Complex and Branches from Actin Filaments. *Curr Biol.* 19:537 – 545.